PAPER

Electronic structure evolution and exciton energy shifting dynamics in WSe$_2$: from monolayer to bulk

To cite this article: Xin Chen *et al* 2021 *J. Phys. D: Appl. Phys.* **54** 354002

View the article online for updates and enhancements.

Electronic structure evolution and exciton energy shifting dynamics in WSe$_2$: from monolayer to bulk

Xin Chen[1]**, Lei Wang**[1,*] , **Hai-Yu Wang**[1,*] , **Xue-Peng Wang**[1]**, Yang Luo**[2] **and Hong-Bo Sun**[1,3]

[1] State Key Laboratory of Integrated Optoelectronics, College of Electronic Science and Engineering, Jilin University, 2699 Qianjin Street, Changchun 130012, People's Republic of China
[2] Changchun Institute of Optics, Fine Mechanics and Physics, Chinese Academy of Sciences, No.3888 Dong Nanhu Road, Changchun 130033, Jilin, People's Republic of China
[3] State Key Laboratory of Precision Measurement Technology and Instruments, Department of Precision Instrument, Tsinghua University, Haidian, Beijing 100084, People's Republic of China

E-mail: lei_wang@jlu.edu.cn and haiyu_wang@jlu.edu.cn

CrossMark

Abstract

Exciton related processes in two-dimensional (2D) transition metal dichalcogenides (TMDCs) play important roles in their optoelectronic applications. In this work, through broadband transient absorption spectroscopy, the electronic band structure evolution, exciton energy shifting dynamics and power-dependence spectral characteristics of WSe$_2$ layers, including monolayer, bilayer, tri-layer and bulk WSe$_2$ under 400 nm and 800 nm excitations are investigated. Particularly, under 400 nm excitation, due to the hot-exciton effect, the A-exciton energy shifting dynamics in WSe$_2$ layers have been analysized in detail, where thicker WSe$_2$ samples possess slower hot-exciton cooling lifetimes, and the exciton recombination approaches are affected by the band structure and interlayer interactions, in comparison with that under 800 nm excitation. The power-dependence spectral evolution in WSe$_2$ layers suggests that the charged states like trions could be facilitated in tri-layer WSe$_2$ (or thicker samples) at the same experimantal conditions. These findings in WSe$_2$ layers could provide a deep insight into the hot-exciton related processes in 2D TMDCs from transient experiments ponit of view.

Supplementary material for this article is available online

(Some figures may appear in colour only in the online journal)

1. Introduction

Two-dimensional (2D) transition metal dichalcogenides (TMDCs), such as WSe$_2$ and MoS$_2$, hold a well-defined bandgap in contrast to the zero gap material of graphene [1–8]. Additionally, due to quantum confinement, these TMDCs usually exhibt an indirect-to-direct bandgap transition as well as bandgap increases when the materials become thinner. This property means that TMDCs have an adjustable bandgap for optoelectronic applications [9]. In addition, as the Coulomb screening effect becomes weaker, the exciton binding energy will be much larger in 2D materials than that in bulk phases. To date, 2D TMDCs have been used to fabricate high performance semiconductor devices, like field-effect transistors (FETs) [10, 11], and photodetectors [12, 13]. Since the

---

J. Phys. D: Appl. Phys. **54** (2021) 354002

X Chen *et al*

exctions mainly determine the absorption, luminescence and transport properties of 2D materials, investigating the exciton related processes could further provide a broader perspective for efficient interconnection between optical data transmission and electronic processing systems [14].

Compared with the reported results for monolayer MoS_2, monolayer WSe_2 exhibits a higher photoluminescence (PL) quantum yield, stronger nonlinear properties, higher carrier mobility and switching ratio [15–18]. Especially, it is reported that 2D WSe_2 has acted as a single photon emitter [19]. There has been a lot of research on the exction behaviors in WSe_2 flakes, which mainly focus on not only the steady-state properties, like absorption, PL, and Raman spectra, but also the exciton dynamics measured by transient absorption (TA) spectroscopy [16–24]. For example, Liu *et al* have been fully reviewed the major methods for the ultrafast carrier dynamics study of 2D TMDCs [24]. However, there is still lack of a comparative study on the electronic structure evolution and exciton energy relaxation processes in WSe_2 layers, which could provide a deep insight into the hot-exciton effect and layer thickness effect on the exciton energy shifting dynamics.

In this work, we investigate the electronic structure evolution, exciton energy relaxation processes and power-dependence spectral characteristics in WSe_2 layers from a transient experiments point of view. Monolayer, bilayer and tri-layer WSe_2 were quasi films, purchased from six-carbon technology (Shenzhen, China) [25]. For bulk WSe_2, fresh flakes are used, obtained by the mechanical exfoliation method [26, 27]. The SEM images of WSe_2 layers are shown in figure S1 (available online at stacks.iop.org/JPD/54/354002/mmedia), presenting relatively smooth surface morphologies. Monolayer, bilayer, tri-layer and bulk WSe_2 are excited and probed by a femtosecond pump–probe system, respectively. Broadband probe pulses ranging from 400 nm to 800 nm are used to measure the TA spectra of samples at different probe times, which record the spectral evolution of ground state bleaching (GSB) signals of excitons. Based on TA analysis, we determine the whole spectral features of the exciton energy shifting in WSe_2 layers under 400 nm and 800 nm excitations, respectively. It shows that as the thickness of WSe_2 increases from monolayer to bulk, a smaller bandgap (red-shift of band-edge GSB signals) and a stronger Coulomb screening (blue-shift of all GSB signals) mainly act together on the spectral evolution of each exciton peak, where the interlayer interactions between odd-layer and even-layer TMDCs also slightly modify the exciton transition energies. Furthermore, under 400 nm excitation, which generates more initial hot-excitons, there is a remarkable hot-exciton effect on the A-exciton energy shifting dynamics of all WSe_2 samples, in compared with that under 800 nm excitation.

2. Materials and methods

2.1. Femtosecond pump–probe system setup

In all TA experiments [40–48], a mode-locked titanium sapphire laser/amplifier system (Solstice, Spectra-Physics) was used. An 800 nm femtosecond pulsed laser with a repetition frequency of 250 Hz is divided into two beams by a splitter. The larger energy beam is incident on the BBO frequency doubling crystal to generate 400 nm excitation light, and the excitation light passes through a chopping wave with a frequency of 125 Hz. The frequency is changed to 125 Hz. After the excitation light is delayed by the delay line (Newport M-ILS250CC), the polarization direction is changed by a half-wave plate, and then the laser beam is focused on the sample. The smaller energy beam of 800 nm light is focused on a nonlinear medium (such as water, sapphire, and CaF_2) to produce super continuum white light, which is then focused on the sample line as the probe light. The position of the excitation light and the probe light on the sample coincide. The probe light through the sample is collected by an Avantes spectrometer [49].

2.2. First-principles calculations

Our DFT [50] calculation employs the projector augmented wave pseudopotential [51], as performed in the VASP code [52]. The electronic exchange–correlation interaction is described by the generalized gradient approximation [53] with the Perdew–Burke–Ernzerhof functional [54]. We use 300 eV as the cutoff energy for the plane wave basis set. The $5 \times 5 \times 1$ Monkhorst–Pack k-points are employed to optimize the structure of monolayer, bilayer and tri-layer WSe_2, while $5 \times 5 \times 2$ k-points are taken for the bulk phase. In the model of monolayer, bilayer and tri-layer WSe_2, a 21.6 Å vacuum layer is used.

3. Results and discussion

To investigate the dependence of band structure on layer thickness, we present the band structures of mono- to tri-layer and bulk WSe_2 initially by first-principles calculations using density functional theory (DFT). As shown in figure 1(a), monolayer WSe_2 exhibits a direct bandgap. Both its conduction band minimum (CBM) and valence band maximum (VBM) locate at the K point. When the thickness of WSe_2 is more than monolayer, the CBM position moves from the K point to the so-called Q/Λ point between the Γ and K points in the reciprocal space (figures 1(b)–(d)). Meanwhile, there is a spin-orbital splitting at the K point for both the conduction band and valence band in all the band structures of WSe_2 layers. Then, in experiment, we distinguish those WSe_2 layers through Raman spectroscopy under a 532 nm excitation, as displayed in figure 1(e). The multiple-peak fitting results and parameters for Raman peaks around E_{2g}^1, A_{1g} and 2LA (M) modes are shown in figure S2 and table S1, respectively. The E_{2g}^1 peak of monolayer WSe_2 located at 252.5 cm^{-1} in Raman specta arises from the in-plane vibrational mode, which is a degenerate state with A_{1g} mode (representing the out-of-plane vibrational mode) in monolayer WSe_2 [16]. As the thickness of WSe_2 layers increases, the E_{2g}^1 and A_{1g} peaks are split out. The 2LA (M) peak (this second-order Raman mode is induced by the LA phonons at point M in the Brillouin zone [16])
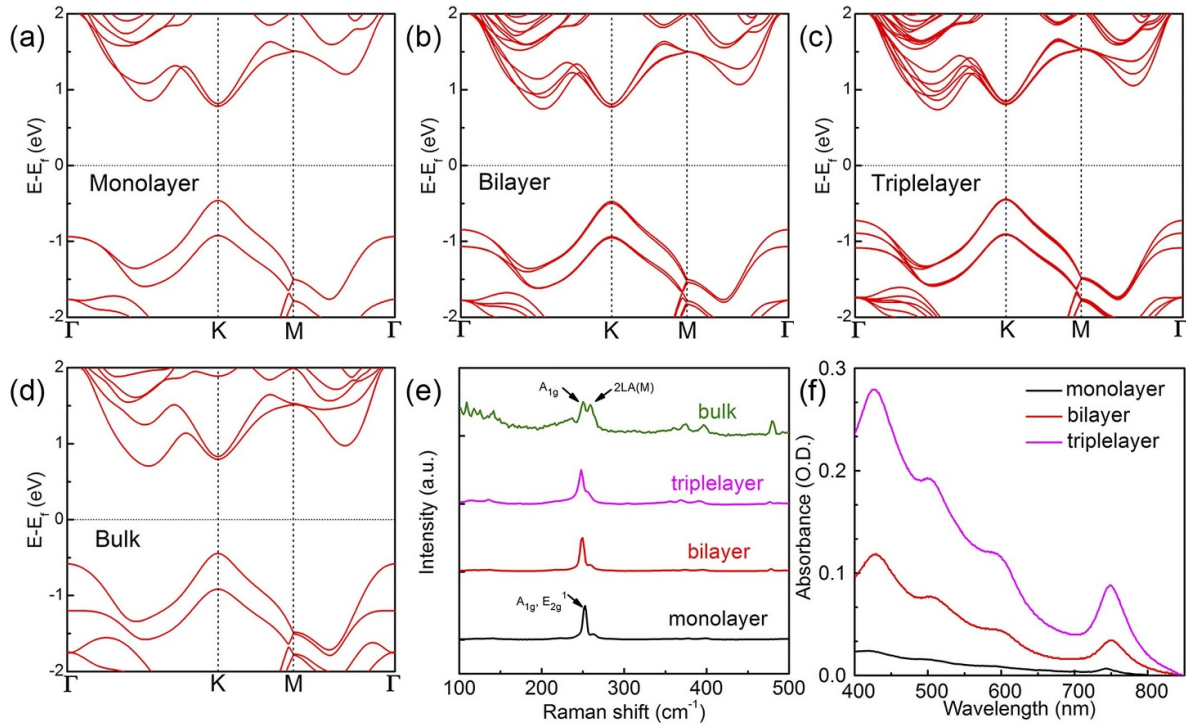
J. Phys. D: Appl. Phys. **54** (2021) 354002

X Chen *et al*

Figure 1. Band structure of monolayer (a), bilayer (b), tri-layer (c), and bulk (d) WSe$_2$ with the most stable stacking order. (e) Raman and (f) steady-state absorbance spectra of monolayer, bilayer, tri-layer, and bulk WSe$_2$.

appearing near the A$_{1g}$ peak locates at 263.4 cm^{-1} in monolayer and red shifts to 259.7 cm^{-1} in bulk.

We also perform the steady-state absorption spectra of WSe$_2$ layers by a Shimadzu UV-2550 UV–VIS scanning spectrophotometer, as shown in figure 1(f). The steady-state absorption peaks of monolayer WSe$_2$ appear at 423 nm, 499 nm, 590 nm, and 743 nm (corresponding to 2.931 eV, 2.485 eV, 2.102 eV and 1.669 eV), which are attributed to C-exciton, A′-exciton, B-exciton and A-exciton transitions, respectively [16, 21, 28–31]. The C-excitons could originate from a parallel band between the conduction band and the valence band [27, 32, 33]. As layer thickness increases, due to the interlayer coupling and quantum confinement effects, the four absorption peaks red shift a little. From high-energy to low-energy excitonic states, it red shifts ∼4 nm, ∼3 nm, ∼1 nm, and ∼5 nm, respectively, when the layer thickness increases from monolayer to tri-layer WSe$_2$. Noting that the absorption peak at 590 nm for all WSe$_2$ layers show a very weak displacement.

In order to shed light on the excited-state evolution processes of band structure and exciton dynamics in WSe$_2$ as a function of layer thickness in the case of band edge excitation, we perform the TA experiments with pump photon energy slightly below the bandgap of WSe$_2$ at 1.55 eV (800 nm) as shown in figures S3(a)–(d), which is trying to avoid the thermal activation of excitons. These TA spectra represent absorption changes measured in the samples after photoexcitation. As shown in figure 2(a), for the TA spectrum of monolayer WSe$_2$, there are four distinct GSB peaks at 424 nm, 507 nm, 594 nm and 747 nm (2.925 eV, 2.446 eV, 2.088 eV and 1.660 eV), which correspond to the four excitons in its
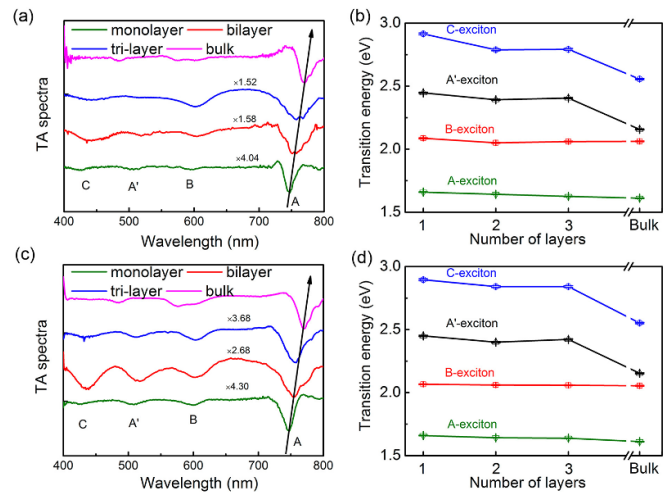

Figure 2. (a) TA spectra of WSe$_2$ probed at ∼0.45 ps from monolayer to bulk under 800 nm excitation. (b) Transition energies of C-, A′-, B-, A-excitons in WSe$_2$ as a function of the number of layers under 800 nm excitation. (c) TA spectra of WSe$_2$ probed at ∼0.45 ps from monolayer to bulk under 400 nm excitation. (d) Transition energies of C-, A′-, B-, A-excitons in WSe$_2$ as a function of the number of layers under 400 nm excitation.

steady-state absorption spectrum. The corresponding transition energy of each exciton state as a function of the number of layers under 800 nm excitation is presented in figure 2(b). It shows a general red shift for the A-exciton state from monolayer to bulk WSe$_2$. For the high-energy exciton states, C- and A′-excitons in WSe$_2$ layers, their transition energies are
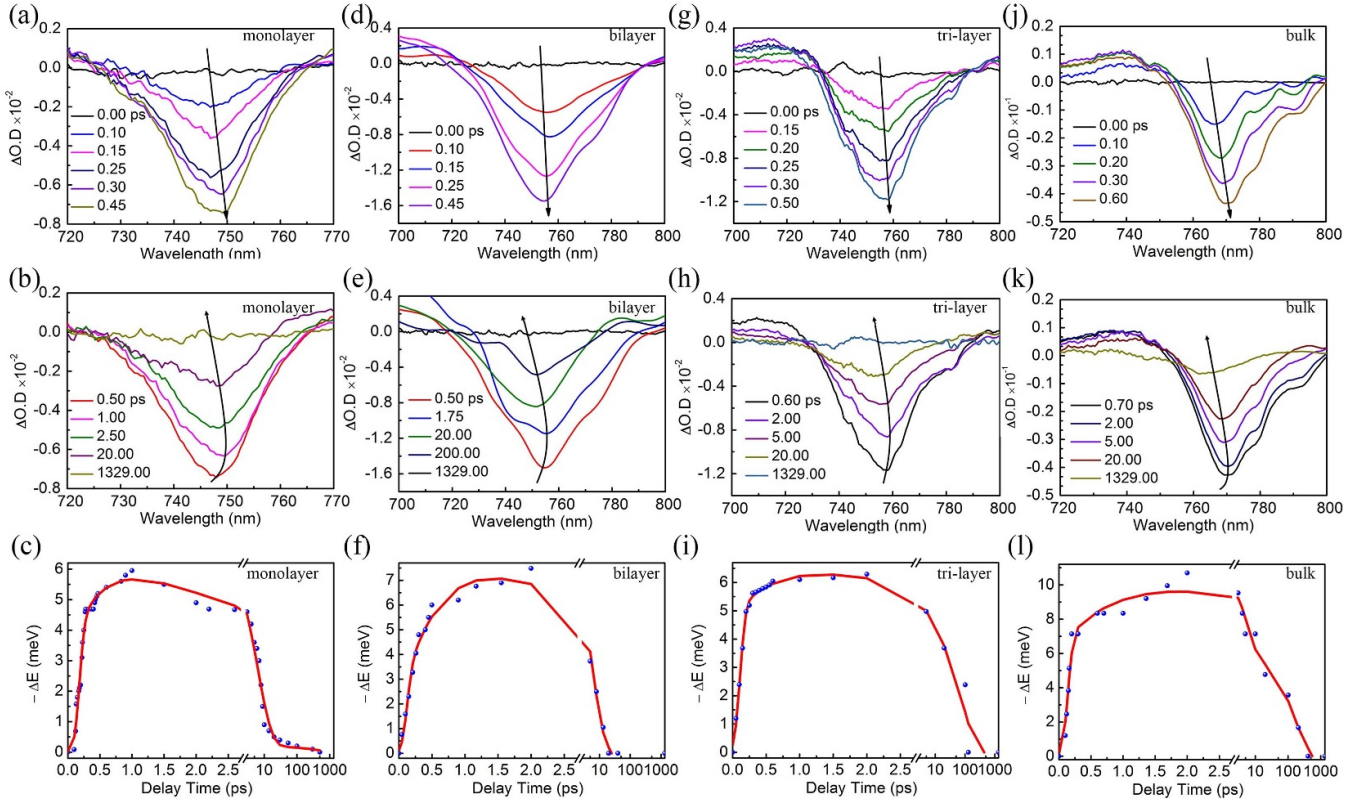
Figure 3. GSB peak evolution of A exciton in monolayer WSe$_2$ under 400 nm excitation (a) within the first 0.45 ps and (b) from 0.5 ps to 1329 ps. (c) Energy shift (ΔE) of A exciton in monolayer WSe$_2$ as a function of delay time. GSB peak evolution of A exciton in bilayer WSe$_2$ under 400 nm excitation (d) within the first 0.45 ps and (e) from 0.5 ps to 1329 ps. (f) Energy shift (ΔE) of A exciton in bilayer WSe$_2$ as a function of delay time. GSB peak evolution of A exciton in tri-layer WSe$_2$ under 400 nm excitation (g) within the first 0.5 ps and from 0.6 ps to 1329 ps (h). (i) Energy shift (ΔE) of A exciton in tri-layer WSe$_2$ as a function of delay time. GSB peak evolution of A exciton in bulk WSe$_2$ under 400 nm excitation (j) within the first 0.6 ps and (k) from 0.7 ps to 1329 ps. (l) Energy shift (ΔE) of A exciton in bulk WSe$_2$ as a function of delay time.

undulately declined, but the B-exciton state seems to be not sensitive to the number of layers.

For comparation, we carry out the TA experiments with pump photon energy above the WSe$_2$ bandgap at 3.1 eV (400 nm) as shown in figures S3(e)–(h). This high-energy excitation is expected to bring the information of hot-exciton effect in this paper. The initial TA spectra for WSe$_2$ layers under 400 nm excitation are show in figure 2(c), where the GSB peaks of monolayer WSe$_2$ appear at 428 nm, 506 nm, 599 nm, and 747 nm (2.897 eV, 2.451 eV, 2.070 eV and 1.660 eV), respectively. Under 400 nm excitation, there are initial hot-exciton population in each exciton state, which would partially affect the initial GSB peak positions, in comparison with that under 800 nm excitation. As layer thickness increases in figure 2(d), the red-shift trends of excitons transition energies for A-, A′-, and C-excitons under 400 nm excitation are also similar to that under 800 nm excitation, and the changes of B-exciton transition energy are very small, too.

There could be three possible reasons for the observed shifts of exciton resonances as the thickness of TMDCs increases: (a) the weakened quantum confinement effect will lead to the decrease of the bandgap [34], that is a decreasing of the exciton transition energy, causing a red shift of the band-edge GSB peak position in TA spectra. (b) The

Coulomb screening effect will be more significant in thicker TMDCs [35], which leads to a larger exciton transition energy and a blue shift of all GSB peaks. (c) The interlayer interaction for TMDCs with odd and even layers could be different [36]. Obviously, the roles of first two effects are against to each other, and the weakened quantum confinement effect is stronger, resulting into the red-shifting trends for A-, A′-, and C-excitons in WSe$_2$ layers; the interlayer interactions between odd-layer and even-layer TMDCs also slightly modify the exciton transition energies. For the B-exciton state in WSe$_2$ layers, the three effects are almost canceled out. Therefore, the GSB peak positions of B-excitons in WSe$_2$ layers are barely changed. There is a significant initial red shift within the first ~0.5 ps followed by a blue shift of the A exciton resonance in all WSe$_2$ layers (figure 3). Take monolayer WSe$_2$ as an example, figures 3(a) and (b) show the whole spectral evolution processes of A exciton, including the peak red-shifting part and peak blue-shifting part, respectively. According to the peak shifting, we could extract the exciton energy shift (ΔE) as a function of delay times presented in figure 3(c). This exciton energy shift dynamics could be divided in three stages for monolayer TMDCs [37], based on our fitting results for the ΔE dynamics. The best-fitted parameters for ΔE of A-exciton in WSe$_2$ layers under 400 nm excitation are presented in table 1.

Table 1. Best-fit parameters for ΔE of A-exciton in WSe$_2$ layers under 400 nm excitation with a function of $I(t) \propto \Sigma_i A_i \exp(-t/\tau_i)$.

	Arising lifetime component	Decay lifetime component	
	τ_1 (ps)	τ_2 (ps)	τ_3 (ps)
Monolayer	0.47 ± 0.10	6.35 (97%)	449 (3%)
Bilayer	0.69 ± 0.11	5.24	
Tri-layer	1.04 ± 0.10	2.01 (57%)	83 (43%)
Bulk	1.25 ± 0.20	3.49 (61%)	160 (39%)
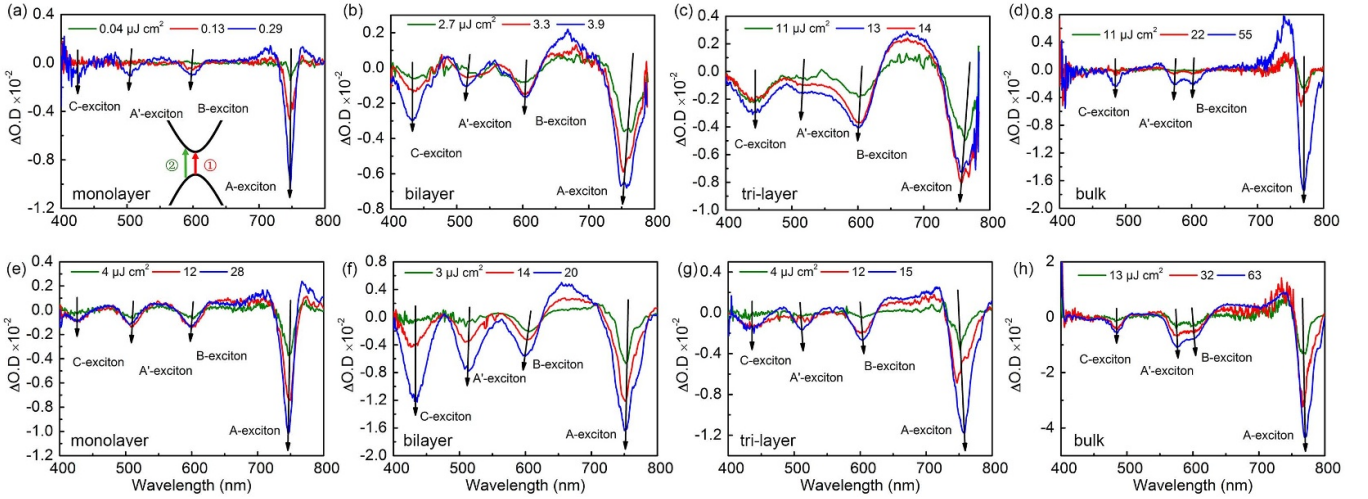
Figure 4. TA spectra of (a) monolayer, (b) bilayer, (c) tri-layer, and (d) bulk WSe$_2$ probed at ∼0.5 ps under 800 nm excitation with different fluences. The inset of panel (a) is the schematic diagram of the band-edge transition processes in WSe$_2$ layers. Process ① represents the transitions at low pump density conditions. Process ② represents the transitions at high pump density conditions. TA spectra of (e) monolayer, (f) bilayer, (g) tri-layer, and (h) bulk WSe$_2$ probed at ∼0.5 ps under 400 nm excitation with different fluences.

Stage ①: the formation of hot excitons within the instrument response function of ∼150 fs. After the high-energy photon (like 3.1 eV) excitation, the hot excitons are rapidly formed due to the large excess energy, which could result in an initially red shift of exciton energy in monolayer WSe$_2$, due to the decreased interexciton distance [37]. Stage ②: the cooling of hot excitons (τ_1, the arising lifetime component). Hot excitons in monolayer WSe$_2$ transfer their excess energies by emitting phonons to the lattice, leading to the following red shift of exciton energy. Stage ③: the recombination of excitons in monolayer WSe$_2$, including the exciton-exciton annihilation (τ_2, the fast decay lifetime component, presenting a power dependent relationship in figure S4) and the recombination of cooled excitons (τ_3, the slow decay lifetime component). The initally high exciton density will decrease quickly by the exciton-exciton annihilation processes (τ_2), which is the main reason for the following blue shift of exciton energy in monolayer WSe$_2$. The recombination appoaches of cooled excitons are responsible for the final blue shift of exciton energy. For monolayer WSe$_2$ with a direct bandgap structure, its τ_3 could be due to the direct recombination of electron–hole pairs, like PL [38].

For few layers and bulk WSe$_2$, the hot-carrier formation mechanism and recombination processes, as shown in figures 3(d)–(l), could be different from monolayer WSe$_2$ due to their indirect bandgap structures. In table 1, it shows that

there is a slower and slower hot-exciton cooling lifetime (τ_1) for thicker WSe$_2$. In stage ③ of bilayer WSe$_2$, it is different from the others, and shows no slow decay lifetime component. It could imply a more efficient Auger recombination in bilayer WSe$_2$. For tri-layer and bulk WSe$_2$, the proportion of exciton-exciton annihilation (τ_2) to the indirect recombination (τ_3) becomes comparable. On the other hand, unlike the 3.1 eV excitation, there is no clear signals for the peak shifting phonomena under the band-edge excitation (1.55 eV) conditions, as shown in figure S5, implying that this hot-exciton effect is not dominant.

Finally, the power-dependence characteristics of spectral evolution in WSe$_2$ layers are investigated. Figures 4(a)–(d) show the TA spectra of WSe$_2$ layers with different pump fluences under the band-edge (1.55 eV) excitation. It shows that all the GSB peaks of A′-, B-, and A-exciton states have a blue shift as the pump fluence increases. This power dependent blueshift of the three GSB peaks could be attributed to the Burstein–Moss filling effect [39], in which the total transition energy of WSe$_2$ is defined as $E_g = E_g^0 + \Delta E_g^{BM}$ (E_g^0 is the intrinsic bandgap of WSe$_2$, and ΔE_g^{BM} is the Burstein–Moss shift). Electrons are mainly excited from the VBM to the CBM as displayed in the inset of figure 4(a) (process ①) when the pump fluences are relatively low. With increasing pump fluences, besides process ①, electrons located in the valence band that lower than the VBM in energy would be excited to the

conduction band that higher than the CBM in energy, namely process ② of the inset of figure 4(a). Therefore, when the pump fluence is large enough, process ② will happen, with a resulting blue shift of the TA peaks as the additional ΔE_g^{BM} for the exciton states will appear. It is worth noting that the initial C-exciton peaks in all WSe_2 layers exhibit almost no power-dependence shifting, probably due to the band-nesting effect. The power-dependence characteristics of spectral evolution in WSe_2 layers under high-energy (3.1 eV) excitation are also performed, as shown in figures 4(e)–(h). All the spectral positions of initial GSB peaks for WSe_2 layers under different pump fluences are presented in table S2. For monolayer and bilayer WSe_2, as the pump fluence of 3.1 eV excitation light increases, the initial GSB peak shifting phenonenon is similar to that under the 800 nm excitation (figures 4(e) and (f)). In contrast, for tri-layer and bulk WSe_2 as shown in figures 4(g) and (h), the GSB peaks of A′-, B-, and A-exciton states exhibit a red-shifting as the pump fluence of 3.1 eV excitation light increases. The reasonable explanation could be the fast formation of low-energy charged states like trions with the help of dissociative free charges in high pump fluences for tri-layer and bulk WSe_2.

4. Conclusions

In summary, we have investigated the electronic band structure evolution and A-exciton energy shift kinetics as a function of WSe_2 layers by femtosecond time-resolved pump–probe spectroscopy. The weakened quantum confinement effect, Coulomb screening effect and the different interlayer interactions for TMDCs with odd and even layers are responsible for the observed changing trends of exciton transition energies in WSe_2 layers. Under 400 nm excitation, we have verified the hot-exciton related energy shifting processes, where thicker WSe_2 possessed slower hot-exciton cooling lifetimes, and the exciton recombination approaches could be affected by the band structure and interlayer interactions, in comparison with that under 800 nm excitation. The power-dependence spectral evolution in WSe_2 layers suggests that the charged states like trions could be facilitated in tri-layer WSe_2 (or thicker samples) with the same experimental conditions.

Data availability statement

All data that support the findings of this study are included within the article (and any supplementary files).

Acknowledgments

Conflict of interest

There are no conflicts to declare.

ORCID iDs

Lei Wang ⬤ https://orcid.org/0000-0003-4304-2887
Hai-Yu Wang ⬤ https://orcid.org/0000-0003-1958-4301
Hong-Bo Sun ⬤ https://orcid.org/0000-0003-2127-8610

References

[1] Geim A K 2009 *Science* **324** 1530
[2] Wu J, Becerril H A, Bao Z, Liu Z, Chen Y and Peumans P 2008 *Appl. Phys. Lett.* **92** 263302
[3] Xia F, Wang H, Xiao D, Dubey M and Ramasubramaniam A 2014 *Nat. Photon.* **8** 899
[4] Psilodimitrakopoulos S, Mouchliadis L, Paradisanos I, Lemonis A, Kioseoglou G and Stratakis E 2018 *Light Sci. Appl.* **7** 18005
[5] Tian H, Chin M L, Najmaei S, Guo Q S, Xia F N, Wang H and Dubey M 2016 *Nano Res.* **9** 1543
[6] Wang Q H, Kalantar-Zadeh K, Kis A, Coleman J N and Strano M S 2012 *Nat. Nanotechnol.* **7** 699
[7] Late D J, Liu B, Matte H S S R, Dravid V P and Rao C N R 2012 *ACS Nano* **6** 5635
[8] Chen K, Wan X and Xu J 2017 *Adv. Funct. Mater.* **27** 1603884
[9] Chen H, Corboliou V, Solntsev A S, Choi D Y, Vincenti M A, De Ceglia D, De Angelis C, Lu Y and Neshev D N 2017 *Light Sci. Appl.* **6** e17060
[10] Vaknin Y, Dagan R and Rosenwaks Y 2020 *Nanomaterials* **10** 2346
[11] Liu W, Cao W, Kang J and Banerjee K 2013 *ECS Trans.* **58** 281
[12] Shen T, Li F, Zhang Z, Xu L and Qi J 2020 *ACS Appl. Mater. Interfaces* **12** 54927
[13] Yang T *et al* 2017 *Nat. Commun.* **8** 1906
[14] Mueller T and Malic E 2018 *Npj 2D Mater. Appl.* **2** 29
[15] Liu W, Kang J, Sarkar D, Khatami Y, Jena D and Banerjee K 2013 *Nano Lett.* **13** 1983
[16] Zhao W, Ghorannevis Z, Amara K K, Pang J R, Toh M, Zhang X, Kloc C, Tan P H and Eda G 2013 *Nanoscale* **5** 9677
[17] Amani M, Taheri P, Addou R, Ahn G H, Kiriya D, Lien D H, Ager J W, Wallace R M and Javey A 2016 *Nano Lett.* **16** 2786
[18] Fang H, Chuang S, Chang T C, Takei K, Takahashi T and Javey A 2012 *Nano Lett.* **12** 3788
[19] Koperski M, Nogajewski K, Arora A, Cherkez V, Mallet P, Veuillen J Y, Marcus J, Kossacki P and Potemski M 2015 *Nat. Nanotechnol.* **10** 503
[20] Zhang X, Qiao X F, Shi W, Wu J B, Jiang D S and Tan P H 2015 *Chem. Soc. Rev.* **44** 2757
[21] Arora A, Koperski M, Nogajewski K, Marcus J, Faugerasa C and Potemski M 2015 *Nanoscale* **7** 10421
[22] Yang J, Xu R, Pei J, Myint Y W, Wang F, Wang Z, Zhang S, Yu Z and Lu Y 2015 *Light Sci. Appl.* **4** e312
[23] Wang G, Bouet L, Lagarde D, Vidal M, Balocchi A, Amand T, Marie X and Urbaszek B 2014 *Phys. Rev.* B **90** 075413
[24] Li Y, Shi J, Mi Y, Sui X, Xu H and Liu X 2019 *J. Mater. Chem.* C **7** 4304
[25] Zheng S W, Wang H Y, Wang L, Wang H and Sun H B 2020 *J. Phys. Chem. Lett.* **11** 9649
[26] Yue Y Y *et al* 2021 *Nanotechnology* **32** 135208

J. Phys. D: Appl. Phys. **54** (2021) 354002

X Chen *et al*

[27] Chen X, Wang Z, Wang L, Wang H Y, Yue Y Y, Wang H, Wang X P, Wee A T S, Qiu C W and Sun H B 2018 *Nanoscale* **10** 9346

[28] Wang Z, Zhao L, Mak K F and Shan J 2017 *Nano Lett.* **17** 740

[29] Manca M *et al* 2017 *Nat. Commun.* **8** 14927

[30] Del Corro E, Terrones H, Elias A, Fantini C, Feng S, Nguyen M A, Mallouk T E, Terrones M and Pimenta M A 2014 *ACS Nano* **8** 9629

[31] Zhao W J, Ghorannevis Z, Chu L Q, Toh M L, Kloc C, Tan P H and Eda G 2013 *ACS Nano* **7** 791

[32] Ramasubramaniam A 2012 *Phys. Rev. B* **86** 115409

[33] Wang L *et al* 2017 *Nat. Commun.* **8** 13906

[34] Gupta A, Sakthivel T and Seal S 2015 *Prog. Mater. Sci.* **73** 44

[35] Chernikov A, Berkelbach T C, Hill H M, Rigosi A, Li Y, Aslan O B, Reichman D R, Hybertsen M S and Heinz T F 2014 *Phys. Rev. Lett.* **113** 076802

[36] Wu Z *et al* 2016 *Nat. Commun.* **7** 12955

[37] Sie E J *et al* 2017 *Nano Lett.* **17** 4210

[38] Palummo M, Bernardi M and Grossman J C 2015 *Nano Lett.* **15** 2794

[39] Manser J S and Kamat P V 2014 *Nat. Photon.* **8** 737

[40] Yan Y J and Mukamel S 1990 *Phys. Rev. A* **41** 6485

[41] Wang L, Chen Q D, Cao X W, Buividas R, Wang X, Juodkazis S and Sun H B 2017 *Light Sci. Appl.* **6** e17112

[42] Wang H, Wang H Y, Chen Q D, Xu H L, Sun H B, Huang F C, Raja W, Toma A and Zaccaria R P 2018 *Laser Photonics Rev.* **12** 1700176

[43] Wang L, Wang H Y, Wei H T, Zhang H, Chen Q D, Xu H L, Han W, Yang B and Sun H B 2014 *Adv. Energy Mater.* **4** 1301882

[44] Liu D X, Sun Y L, Dong W F, Yang R Z, Chen Q D and Sun H B 2014 *Laser Photonics Rev.* **8** 882

[45] Arain Z, Liu C, Yang Y, Mateen M, Ren Y, Ding Y, Liu X, Ali Z, Kumar M and Dai S 2019 *Sci. China Mater.* **62** 161

[46] Peng H and Tan Z 2018 *Sci. China Mater.* **61** 1017

[47] Omair Z, Pazos-Outon L M, Steiner M A and Yablonovitch E 2020 *PhotoniX* **1** 21

[48] Zhao R, Huang L and Wang Y 2020 *PhotoniX* **1** 20

[49] Siddique R H, Mertens J, Holscher H and Vignolini S 2017 *Light Sci. Appl.* **6** e17015

[50] Hohenberg P and Kohn W 1964 *Phys. Rev. B* **136** 864

[51] Blochl P E 1994 *Phys. Rev. B* **50** 17953

[52] Kresse G and Furthmüller J 1996 *Phys. Rev. B* **54** 169

[53] Perdew J P and Yue W 1986 *Phys. Rev. B* **33** 8800

[54] Perdew J P, Burke K and Ernzerhof M 1996 *Phys. Rev. Lett.* **77** 3865